Composite state control and magnetic properties of Co and Si cluster assemblies prepared with double-glow-discharge sources

Ryoji Katoh,[a] Takehiko Hihara, Dong-Liang Peng, and Kenji Sumiyama
Department of Materials Science and Engineering, Nagoya Institute of Technology, Nagoya 466-8555, Japan

(Received 7 December 2005; accepted 17 May 2006; published online 7 August 2006)

Using a double-glow-discharge-cluster-source system, in which one glow discharge was a dc mode and the other an rf discharge mode, Co and Si clusters were independently produced and simultaneously deposited on a substrate. When a separation plate was inserted between two glow-discharge chambers, a mixture of Co and Si clusters was obtained: small Co clusters were distributed at random, while the Si clusters were aggregated to form large secondary particles. Without inserting the separation plate, on the other hand, core-shell clusters were obtained: a Co core was surrounded by small Si crystallites. The magnetization measurement indicated that the magnetic coercive force of Co/Si core-shell cluster assemblies was much smaller than that of Co cluster assemblies in which Co clusters were covered with antiferromagnetic CoO shells, indicating that the Si shell prevented Co cluster surfaces from their oxidation. Therefore, the present double-cluster-source system is useful in fabricating various sorts of cluster composites, which cannot be prepared by conventional coevaporation or precipitation methods. © *2006 American Institute of Physics*. [DOI: 10.1063/1.2219699]

I. INTRODUCTION

Cluster assembling is a unique method for fabricating nanoscale structure-controlled materials.[1] In order to utilize the size-dependent characteristics of nanoclusters, we have to make regular size clusters and to prevent their oxidation and intercluster aggregation. Using a plasma-gas-condensation (PGC)-type cluster deposition system, we have succeeded in preparing monodispersive size transition metal clusters whose mean diameters d range between 6 and 15 nm with the standard deviation less than 10% of d.[2] With increasing the deposition time of such clusters on a substrate, only the number of clusters increases while their initial sizes are maintained. We have clearly observed geometrical and electrical percolation phenomena[3] and a transition from superparamagnet to ferromagnet at a certain critical deposition thickness.[4] When we introduce a very small amount of oxygen gas into the deposition chamber, the surfaces of transition metal clusters are uniformly oxidized.[5] Such core-shell clusters are stable against oxidation in ambient atmosphere and prohibit the direct contact and coalescence of metallic cores. The core-shell-type monodisperse Co/CoO cluster assemblies thus obtained reveal tunneling-type electrical resistivity and magnetoresistance[5] and a macroscopic quantum-tunneling-type magnetic relaxation at low temperatures,[6] where these characteristic features can be well distinguished from the normal semiconductor-type conductivity and classical magnetic relaxation at high temperatures.

Moreover, it has been reviewed that impinged atoms and microclusters migrate on a substrate even at ambient temperature.[1] This feature is attributed to the enhanced diffusion of surface atoms in clusters, surface melting of clusters, and defect-induced diffusion of clusters.[7] In such supported clusters, one of the spectacle features is spontaneous alloying:[8] discontinuous metal islands formed on a substrate by thermal evaporation accumulate impinging metal atoms supplied by postevaporation and become homogeneous alloy islands as long as their sizes are less than 10 nm in diameter. In this paper, we describe various sorts of cluster assemblies obtained by the independent formation of Co and Si clusters with controlling their collision time and simultaneous deposition.[9] We also mention the magnetic properties of these Co/Si cluster assemblies.

II. EXPRIMENTAL PROCEDURES

A double source plasma-gas-condensation cluster deposition system was made from a previous co-sputter-deposition apparatus, which had a couple of facing target-type sputtering chambers being used for preparing alloy films.[10] One cluster source system was operated with a dc glow discharge mode for preparing metal clusters and another with an rf glow discharge mode for preparing semiconductor and insulator clusters. As shown in Fig. 1, sputter (glow-discharge) chambers 1A and 1B and a deposition chamber 3 are separated by the air-tight wall and indirectly connected via a growth duct 2. A separation plate can be placed and removed between chambers 1A and 1B, where the vacuum conditions of both chambers are almost the same. Since a high gas atmosphere (from 0.1 to 0.2 kPa) was necessary for the nucleation and growth of clusters in a gas phase, we reduced the target-shield distance to prohibit a corona discharge.[11] A large amount of Ar gas (99.9999 vol %) was introduced through gas inlets with variable leak valves whereas chambers 1A and 1B and duct 2 were evacuated via chamber 3 by a mechanical booster pump (500 m^3/h) to eject the Ar gas, sputtered atoms, and formed

[a]Electronic mail: ryoji@ss.emat.nitech.ac.jp

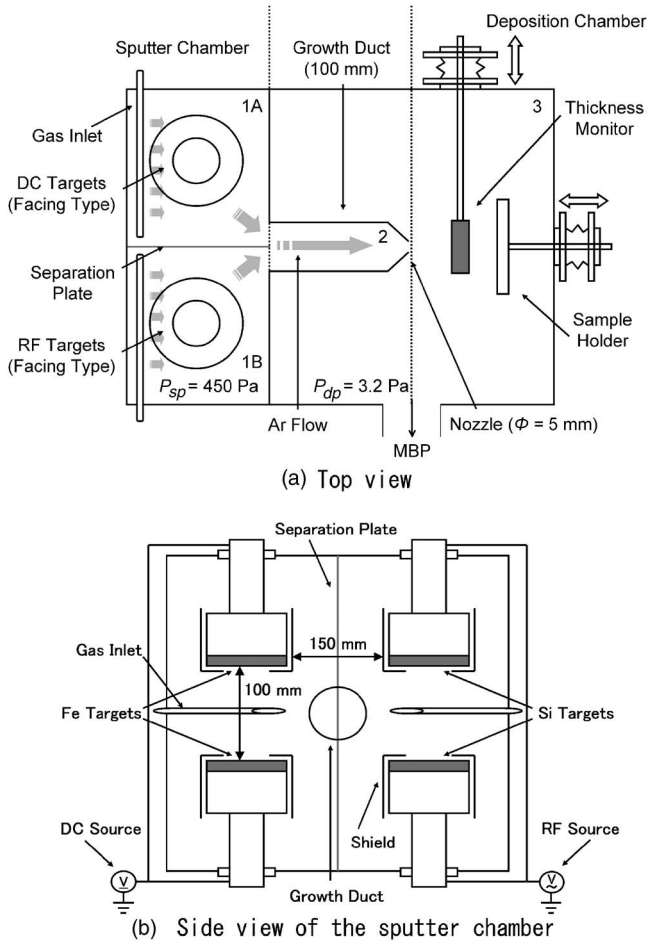

FIG. 1. Schematic drawing of double source plasma-gas-condensation apparatus: (a) top and (b) side views of the apparatus.

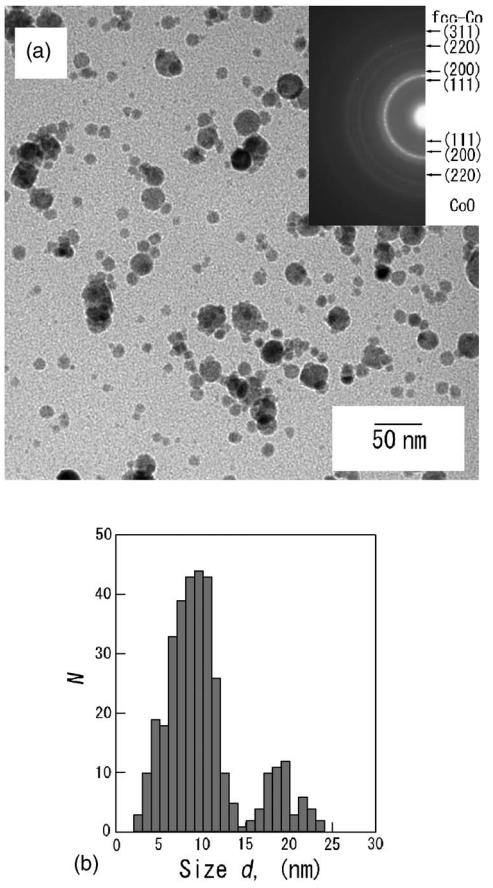

FIG. 2. (a) Bright field TEM image of Co clusters prepared by the dc glow discharge with the electric power of 250 W. (b) The size distribution histogram of Co clusters estimated from Fig. 2(a).

clusters through the small nozzle, where the Ar gas flow rate $R_{\mathrm{Ar}}=2.5\times10^{-6}$ m^3/s corresponded to the Ar gas pressure in chambers 1A and 1B, $P_{\mathrm{sp}}=450$ Pa.

When the dc plasma was well controlled, the plasma sheath was confined near the targets even above 300 W. On the contrary, the rf plasma was rather unstable in such a high Ar gas pressure and the sheath could not be confined near the targets. A corona discharge was often observed when the rf electric power was higher than 300 W. When both the dc and rf glow discharges were simultaneously supplied and the electric power of the rf discharge was higher than 180 W, the rf and dc discharges often interfered with each other and the glow discharges became unstable. Therefore, we fixed the rf power at 150 W and changed the dc power between 180 and 300 W to vary the mixing ratio of Co clusters to Si clusters.

The morphology, size, and structure of Co, Si, and Co/Si clusters were observed using a transmission electron microscope (TEM) (Hitachi Co., HF-2000) operating at 200 kV. TEM images were observed for the specimens at the initial deposition stage and electron diffraction patterns for those at the late deposition stage. The chemical compositions of Co and Si were determined by an energy dispersive x-ray (EDX) analyzer installed in TEM, where the O content was neglected owing to the quantitative resolution limit. Magnetization curves for the Co/Si cluster assemblies deposited on polyimide film substrates were measured by a superconducting quantum interface device magnetometer (Quantum Design Co., MPMS-5) applying a magnetic field of up to 1600 kA m^{-1}.

III. RESULTS

A. Single source experiment

Figures 2(a) and 2(b) show the TEM image and the size distribution of Co clusters deposited on a TEM grid by the dc glow discharge with the electric power of 250 W. There are various size clusters whose distribution reveals double peaks. The smaller peak corresponds to independently deposited clusters and the larger one to coalesced clusters, because the present system could not exclude the deposition of very small clusters which migrated and merged to other clusters on the substrate. With the increase in R_{Ar} (P_{sp}), the average Co cluster size increases and the size distribution becomes wider. With the increase in the dc electric power, the average cluster size also increases, being ascribed to the increase in vaporized atoms with the electric power. The diffraction patters of the Co cluster assemblies are indexed as fcc Co and CoO structures. With decreasing the size of Co clusters to nanoscale, the fcc structures appear instead of the hcp structures.[4] Since every observation and evaluation of the cluster assemblies is going after aeration in an ambient atmosphere, the surface of the Co clusters are oxidized.

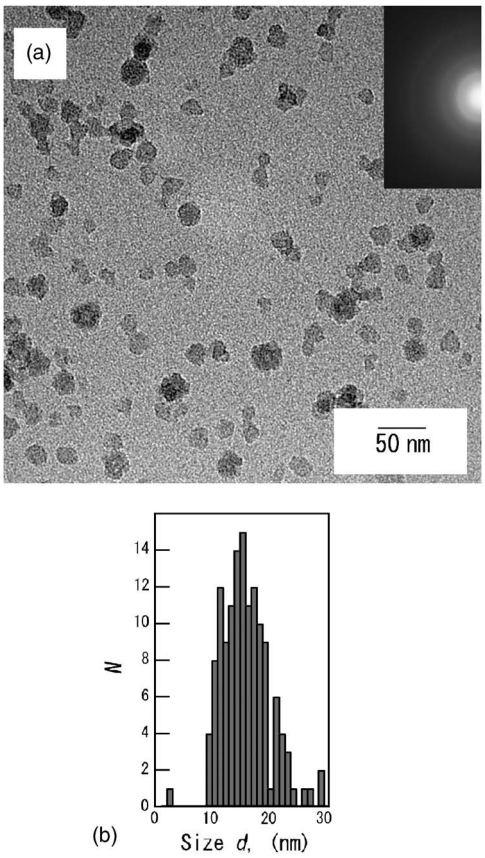

FIG. 3. (a) Bright field TEM image of Si clusters prepared by the rf glow discharge with the electric power of 150 W. (b) The size distribution histogram of Si clusters estimated from Fig. 3(a).

Figures 3(a) and 3(b) show the TEM image and the size distribution of Si clusters deposited on a TEM grid by the rf glow discharge with the electric power of 150 W. The average cluster size of Si clusters is larger than that of Co clusters even though the electric power is lower than that for the Co cluster preparation. The shapes of Si clusters are irregular and the size distribution is of a log-normal type, also indicating cluster coalescence. In the electron diffraction (ED) patterns, there is no crystal-diffraction line but there are weak halo rings corresponding to an amorphous Si and/or the carbon grid.

B. Double source experiment with inserting the separation plate

Figures 4(a) and 4(b) show the TEM images of Co/Si composite clusters deposited on TEM grids at the dc electric powers of 250 W with inserting the separation plate between the chambers 1A and 1B. Figure 4(a) is the result for a high cluster density region and Fig. 4(b) that for a low cluster density region. The average chemical composition of the Co/Si composite cluster assembly is 94 at. % Co. Since the chemical compositions of regions A and B in Fig. 4(b) were determined to be 4 at. % Co and 91 at. % Co, respectively, small clusters are Co rich and the large aggregates to Si rich ones. Figure 5 shows the electron diffraction pattern of the Co/Si composite cluster assembly. In order to determine crystal structures of Co/Si composite cluster assemblies prepared with a separation plate, we made a thin filmlike specimen whose average chemical composition was 42 at. % Co, which consists of fcc Co rings (a=0.354 nm) and broad halo rings overlapping with (111) and (200) lines of fcc Co. There are weak diffraction rings corresponding to a CoO phase (a =0.426 nm), while there is no diffraction line corresponding to Co–Si compounds.

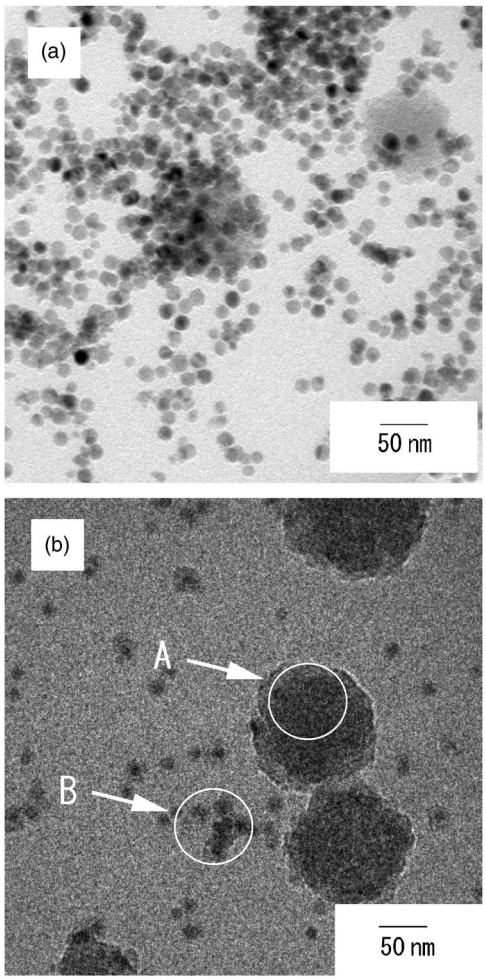

FIG. 4. Bright field TEM images of Co/Si composite clusters prepared by dc and rf glow discharge modes with inserting the separation plate between two chambers, 1A and 1B. (a) The TEM image for a high cluster density region and (b) that for a low cluster density region. The chemical composition of region A is 4 at. % Co and that of region B is 91 at. % Co. The average chemical composition of these clusters is 94 at. % Co.

Figures 6(a) and 6(b) show the magnetization curves at 300 and 5 K for a Co/Si composite cluster assembly with the average chemical composition of 87 at. % Co prepared at the dc electric power of 200 W. The magnetization is easily saturated at both 300 and 5 K, indicating that the specimen is ferromagnetic. The magnetic coercive force H_C is very small, about 2.5 kA/m at 300 K and about 22 kA/m at 5 K. Figure 7 shows the zero-field-cooled and field-cooled thermomagnetic curves of the same Co/Si composite cluster assembly in a magnetic field of 8 kA/m. These gradual temperature variations suggest that the magnetic interactions between Co clusters are strong, consistent with ferromagnetic behavior at 300 K in Fig. 6(a).

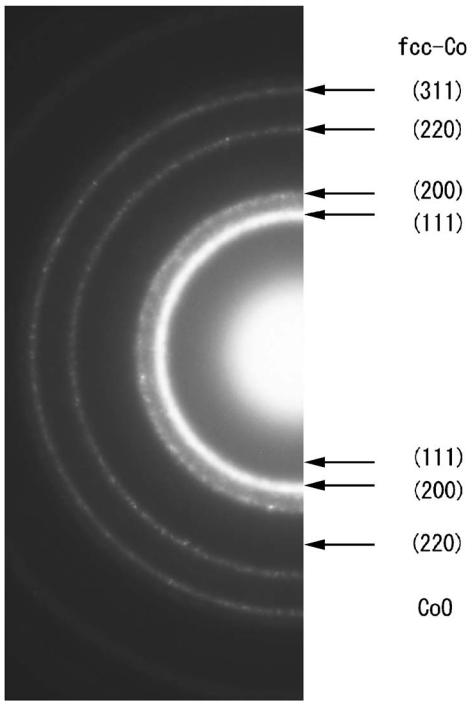

FIG. 5. A selected area electron diffraction pattern of Co/Si composite clusters deposited on a carbon microgrid by dc and rf glow discharge modes with inserting the separation plate between two chambers, 1A and 1B. The average chemical composition of the cluster assembly is 94 at. % Co.

C. Double source experiment without inserting the separation plate

Figures 8(a)–8(c) show TEM images of Co/Si core-shell cluster assemblies prepared at the dc electric powers of 300, 250, and 180 W without inserting the separation plate between the chambers 1A and 1B. The average chemical compositions of these cluster assemblies are 98, 37, and 28 at. % Co. As seen in these figures, the dark contrast clusters are surrounded by the gray contrast clusters, and the volume fraction of the former tends to increase with increasing dc electric power. Figure 9 shows the TEM image of Co/Si core-shell cluster assemblies prepared at the dc electric powers of 250 W. The chemical composition of a dark contrast core region (marked by A) is about 45 at. % Co and that of a gray contrast shell region (marked by B) is about 18 at. % Co, whereas the average composition of these clusters is about 22 at. % Co. Figure 10 shows the electron diffraction pattern of a Co/Si core-shell cluster assembly with the average chemical composition of 37 at. % Co prepared at the dc electric power of 250 W. It reveals diffused fcc rings (attributable to Co clusters), broad halo rings (attributable to Si clusters), and no diffraction ring corresponding to CoO. Owing to the contamination effect, we could not find out whether Co and Si are mixed in an atomic scale to form a primary solid solution and/or an amorphous phase. However, these results clearly demonstrate that a core-shell-type morphology is obtained when Co/Si cluster assemblies are prepared without inserting the separation plate.

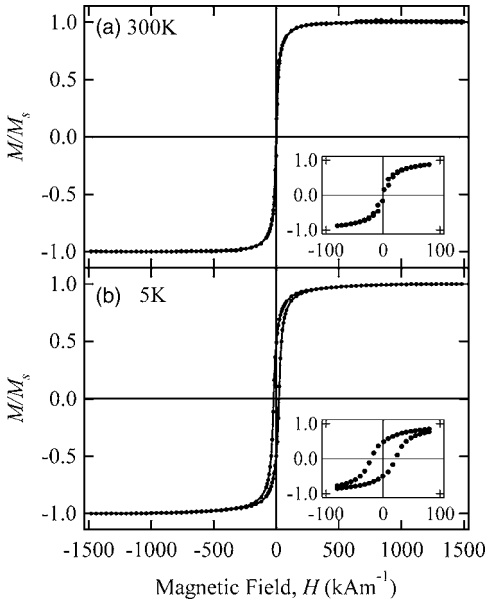

FIG. 6. Magnetization curves at (a) 300 and (b) 5 K for a Co/Si composite cluster assembly with the average chemical composition of 87 at. % Co. The low-field region is shown in the inset.

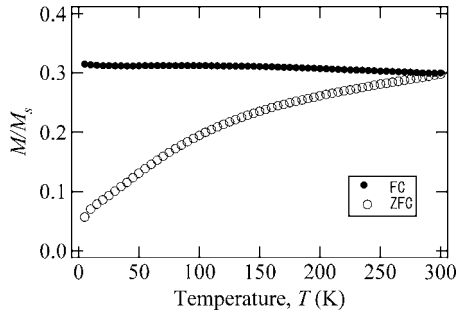

FIG. 7. Thermomagnetic curves measured under the applied magnetic field of 8 kA/m for zero-field-cooled (ZFC) and field-cooled (FC) states of a Co/Si composite cluster assembly with the average chemical composition of 87 at. % Co.

Figures 11(a) and 11(b) show the magnetization curves at 300 and 5 K for a Co/Si core-shell cluster assembly whose chemical composition is 37 at. % Co prepared at the dc electric power of 250 W. The magnetization is not so easily saturated at 300 and 5 K in comparison with those in Fig. 6, indicating that the specimen contains superparamagnetic particles. H_C is about 3.0 kA/m at 300 K and about 59 kA/m at 5 K. Figure 12 shows the zero-field-cooled and field-cooled thermomagnetic curves of the same sample. In Fig. 12, the temperature gradients become larger at low temperatures in both the zero-field-cooled and field-cooled specimens, indicating that magnetic couplings between Co clusters are weak.

IV. DISCUSSION

A. Morphology and structure of Co/Si clusters

The sizes of present Co clusters are not monodispersed in comparison with those prepared by using our previous single-cluster-source PGC system in which several differentially pumped chambers were connected to carry clusters into higher vacuum spaces and minimize their aggregation.[2,3] In the present experiment, where P_{sp}(=450 Pa) is much higher than P_{sp}=100 Pa of the previous system, clusters and vapor-

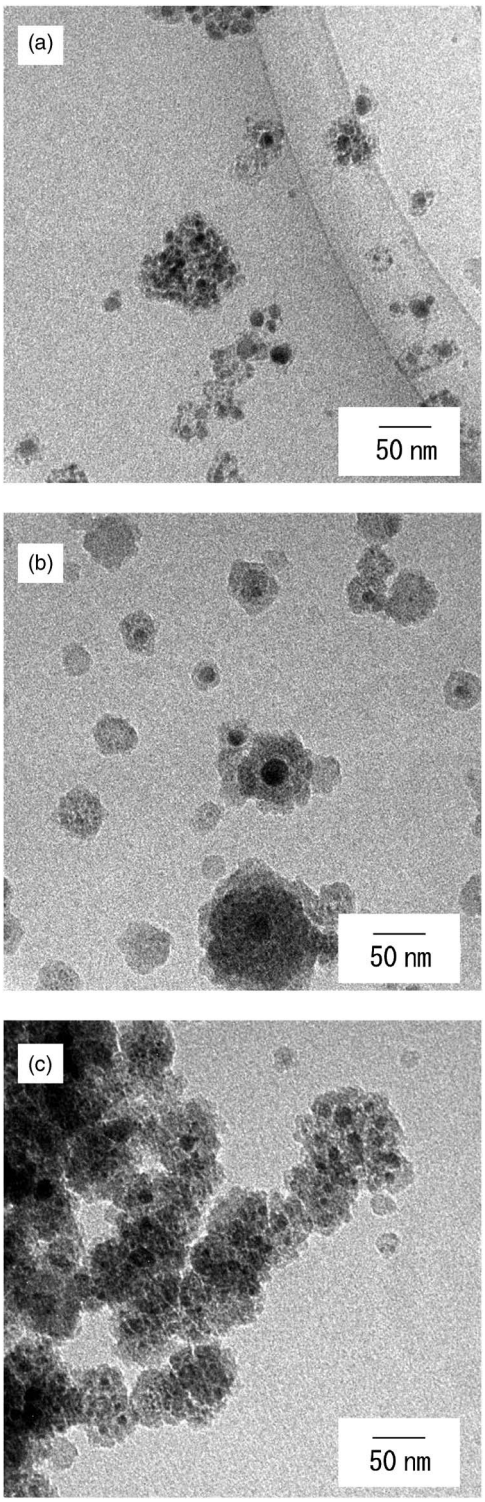

FIG. 8. Bright field TEM images of Co/Si core-shell clusters prepared by dc and rf glow-discharge modes without inserting the separation plate between two chambers, 1A and 1B. Their average chemical compositions are (a) 98 at. % Co, (b) 37 at. % Co, and (c) 28 at. % Co.

ized atoms are prolonged to collide with each other, leading to a wide cluster size distribution. Moreover, since the transportation path from the cluster source to the deposition chamber in the previous system (about 750 mm) was much longer than that in the present system (350 mm), smaller clusters were scattered out and not deposited on the substrate, leading to a size selection of larger clusters.

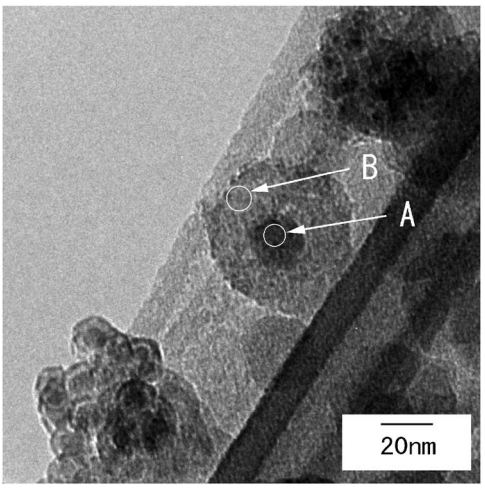

FIG. 9. Bright field TEM image of Co/Si core-shell clusters. The chemical composition of region A is about 45 at. % Co and that of region B is about 18 at. % Co, whereas the average chemical composition of these cluster assemblies is 22 at. % Co.

The sizes of Si clusters are larger than those of Co clusters, and the shapes of Si clusters are irregular and not spherical as shown in Fig. 3. The size distribution curves are of a log-normal type. The apparently large Si clusters are secondarily aggregated ones of primary Si clusters,[12] probably because the aggregation is enhanced due to dangling bonds in primary Si clusters and/or oxidation by remaining O_2 gas. Since these clusters are thermalized in the early stage of nucleation, the reconstruction of Si atoms and their coalescence are restrained in large Si clusters.

When Co and Si clusters were prepared independently with inserting the separation plate between the chambers 1A and 1B, the vaporized atoms and formed cluster nuclei are very quickly cooled in such a high Ar gas atmosphere, mixed in the duct 2, and simultaneously deposited on the substrate. In the equilibrium phase diagram of Co–Si system,[13] Co

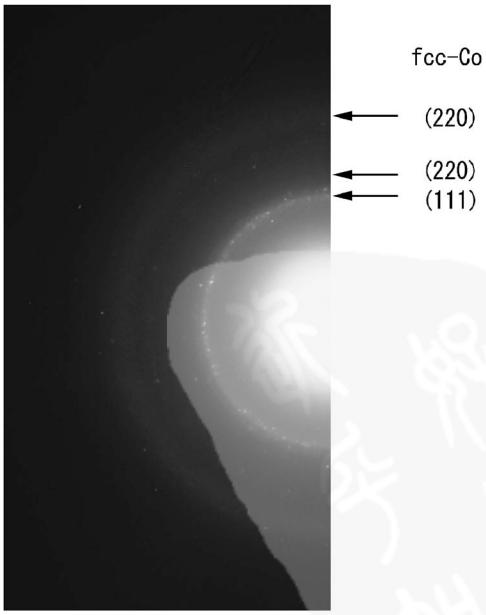

FIG. 10. A selected area electron diffraction pattern of a Co/Si core-shell cluster assembly with the average chemical composition of 37 at. % Co.

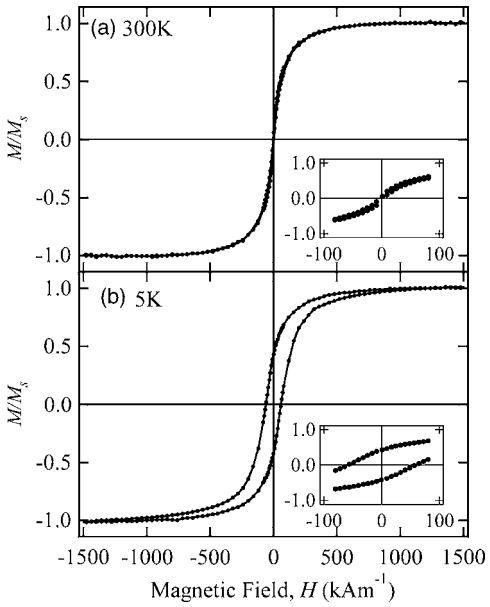

FIG. 11. Magnetization curves at (a) 300 and (b) 5 K for a Co/Si core-shell cluster assembly with the average chemical composition of 37 at. % Co. The low-field region is shown in the inset.

forms the primary solid solution up to 16 at. % Si at about 1500 K, while Si forms almost no primary solid solution up to 1700 K. Since the Co- and Si-cluster sizes are also larger than the critical size of about 10 nm for the occurrence of the instantaneous alloying,[8] it is reasonable that fcc Co and amorphous Si clusters coexist on the substrate.

Since the Co and Si targets are at intervals of 150 mm (see Fig. 1), vaporized Co and Si atoms form cluster nuclei and grow independently without the separation plate. When these cluster nuclei are mixed before they enter the duct 2, Co- and Si-cluster nuclei collide with each other. Since the surface tension of Si is much lower than that of Co,[14] Si clusters cover Co cluster surfaces to form the core-shell clusters, suppressing the coalescence and growth of Co clusters, where the slight mixing and alloying of Co and Si clusters cannot be excluded due to the limitation of nanoscale structural and chemical analyses. The immiscible characters are quite different from our previous experiment in which we obtained homogeneously alloyed clusters using the single dc glow-discharge source.[15,16] In the equilibrium phase diagram, moreover, Co and Si form very stable intermetallic compounds, CoSi, Co_2Si, and $CoSi_2$,[13] indicating that their formation enthalpies are negative and their absolute values are so large that Co–Si alloy clusters have been expected in contrast to the present results. Indeed, there have been a lot of reports on the instantaneous alloying of nanoscale islandlike clusters on substrates with postdeposited atoms at ambient temperature[8] and silicides were formed when islandlike Co films were deposited on a silicon substrate and annealed above 700 K.[17] Moreover, Co silicidation has been used as an interconnect for very large scale integrated (VLSI) devices. When Co atoms were deposited on the cleaned Si substrate, the formation of Co silicides was enhanced by the absorption of Co atoms on particular sites of a Si surface in room temperature.[18] Whereas on the oxidized and H atom terminated Si surfaces,[19,20] on the other hand, the Co silicidation was suppressed at room temperature but without thermal annealing. In our experiment, Co and Si clusters and their nuclei collide with each other in the duct 2 and/or on the substrate. Even though, intercluster atom diffusion is suppressed and Co and Si clusters do not coalesce to form alloy clusters at their contact and/or collision events. In order to explain the present results, we have to take into account of the vacuum condition (0.1 Pa) of the cluster deposition chamber being about three orders of magnitude larger than the previous experiment.[2,21] If chemically active Si cluster surfaces are oxidized by O_2 impurity, the alloying of Si with Co are severely suppressed.

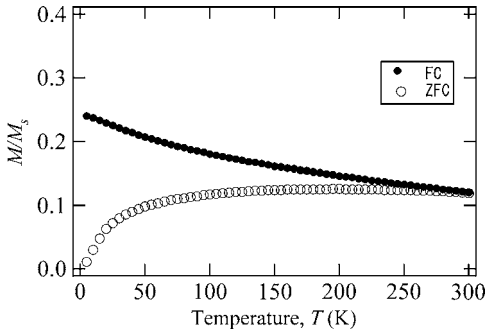

FIG. 12. Thermomagnetic curves measured under the applied magnetic field of 8 kA/m for zero-field-cooled (ZFC) and field-cooled (FC) states of a Co/Si core-shell cluster assembly with the average chemical composition of 37 at. % Co.

B. Magnetic properties of Co/Si cluster assemblies

The magnetic properties of present Co/Si cluster assemblies are discussed in comparison with that of Co cluster assemblies. The enhancement of magnetic coercivity in Co cluster assemblies has been ascribed to the surface oxidation of Co clusters because CoO oxide layers are antiferromagnetic, yielding strong exchange coupling with ferromagnetic Co core.[6] Since the irregular interfaces between Co cores and CoO shells give rise to spin-glass-like random anisotropy which disturbs the alignment of Co core moment along the applied field direction.[22–24] The magnetization curves shown in Figs. 6 and 11, however, indicate that the magnetic coercivity of Co/Si cluster assemblies prepared both with and without inserting the separation plate are much smaller than those of simple Co cluster assemblies.[22] This character is more marked at 5 K. As shown in the electron diffraction patterns, the diffraction rings attributed to CoO are slightly detected in Fig. 5 but not in Fig. 10. These results suggest that the Co/Si core-shell cluster assemblies are not easily oxidized in ambient atmosphere.

The present Co/Si composite cluster assemblies are porous and the magnetic interaction between Co clusters is of a magnetic dipole type, resulting in weak random anisotropy.[22] It is worth comparing the thermomagnetic curves of zero-field-cooled states between the Co/Si cluster assemblies prepared with and without inserting the separation plate. In Fig. 7, the M/M_s value [field cooled (FC)] monotonically increases with T, suggesting that the sizes of Co clusters are widely distributed due to agglomeration. In Fig. 12, on the other hand, it rapidly varies at low temperatures, revealing a

more marked convex curve. This feature and the nonsaturation behavior in Fig. 11 suggest that the Co/Si core-shell cluster assembly has a superparamagnetic character probably because Si shells interrupt the magnetic interaction between Co clusters.

V. CONCLUSION

We have obtained simple mixtures of Co and Si clusters when they are independently formed and mixed in the later stage while core-shell clusters when they are also independently formed but mixed with each other in the early stage. At the present, we cannot explain the immiscibility between nanometer size Co and Si clusters. However, these unique results suggest the forming ability of various sorts of Co and Si nanocomposite materials using the present double-cluster-source system. In particular, core-shell clusters are promising for use as stable nanobuilding blocks.

ACKNOWLEDGMENTS

The authors thank K. Wakoh for his experimental suggestion and K. Tsunoda for his experimental assistance. This work has been supported by (1) Intellectual Cluster Project supported by the Ministry of Education, Science, Sports, and Culture of Japan, Aichi Prefecture, Nagoya City, and Aichi Science and Technology Foundation, (2) a Grant-in-Aid for Scientific Research given by the Ministry of Education, Culture, Sports, Science, and Technology of Japan (MEXT), (3) NITECH 21st Century COE Program "World Ceramics Center for Environmental Harmony," (4) the Research Encourage Program of our University, and (5) Kato Society of Science Promotion.

[1]P. Melinon *et al.*, Int. J. Mod. Phys. B **9**, 339 (1995).
[2]S. Yamamuro, K. Sumiyama, and K. Suzuki, J. Appl. Phys. **85**, 483 (1999).
[3]S. Yamamuro, K. Sumiyama, T. Hihara, and K. Suzuki, J. Phys.: Condens. Matter **11**, 3247 (1999).
[4]S. Yamamuro, K. Sumiyama, T. J. Konno, and K. Suzuki, Mater. Trans., JIM **40**, 1450 (1999).
[5]D. L. Peng, T. J. Konno, K. Wakoh, T. Hihara, and K. Sumiyama, Appl. Phys. Lett. **78**, 1535 (2001); D. L. Peng, K. Sumiyama, T. J. Konno, T. Hihara, and S. Yamamuro, Phys. Rev. B **60**, 2093 (1999).
[6]D. L. Peng, K. Sumiyama, S. Yamamuro, T. Hihara, and T. J. Konno, Appl. Phys. Lett. **74**, 76 (1999); D. L. Peng, K. Sumiyama, T. Hihara, S. Yamamuro, and T. J. Konno, Phys. Rev. B **61**, 3103 (2000).
[7]P. Jensen, Rev. Mod. Phys. **71**, 1695 (1999).
[8]H. Mori, M. Komatsu, K. Takeda, and H. Fujita, Philos. Mag. Lett. **63**, 173 (1991); H. Yasuda and H. Mori, Phys. Rev. Lett. **69**, 3747 (1992).
[9]R. Katoh, T. Hihara, D. L. Peng, and K. Sumiyama, Appl. Phys. Lett. **82**, 2688 (2003).
[10]T. J. Konno, K. Shoji, K. Sumiyama, and K. Suzuki, J. Magn. Magn. Mater. **195**, 9 (1999).
[11]H. Haberland, M. Mall, M. Moseler, Y. Qiang, T. Reiners, and Y. Thurner, J. Vac. Sci. Technol. A **12**, 2925 (1994).
[12]C. G. Granqvist and R. A. Buhrman, J. Appl. Phys. **47**, 2200 (1976).
[13]T. B. Massalski, J. L. Murray, L. H. Bennett, H. Baker, and L. Kacprzak, *Binary Alloy Phase Diagrams*, 2nd ed. (American Society of Metals, Metals Park, OH, 1990), p. 1238.
[14]F. R. de Boer, R. Boom, W. C. Mattens, and A. R. Miedema, *Cohesion in Metals—Transition Metal Alloys* (North-Holland, Amsterdam, 1988), p. 662.
[15]T. J. Konno, S. Yamamuro, and K. Sumiyama, J. Appl. Phys. **90**, 3079 (2001); J. Vac. Sci. Technol. A **20**, 834 (2002).
[16]D. L. Peng, T. Hihara, and K. Sumiyama, Appl. Phys. Lett. **83**, 350 (2003).
[17]C. Calandra, O. Bisi, and G. Ottaviani, Surf. Sci. Rep. **4**, 271 (1985).
[18]V. Scheuch, B. Voigtländer, and H. P. Bonzel, Surf. Sci. **372**, 71 (1997).
[19]G. Palasantzas, B. Ilge, J. de Nijs, and L. J. Geerligs, Surf. Sci. **412/413**, 509 (1998).
[20]K. Sakamoto, T. Maeda, and M. Hasegawa, Thin Solid Films **369**, 204 (2000).
[21]T. Hihara and K. Sumiyama, J. Vac. Sci. Technol. B **17**, 1923 (1999).
[22]S. Yamamuro, K. Sumiyama, T. Kamiyama, and K. Suzuki, J. Appl. Phys. **86**, 5726 (1999).
[23]D. L. Peng, K. Sumiyama, and T. Hihara, Jpn. J. Appl. Phys., Part 1 **39-P1**, 66 (2000).
[24]D. L. Peng, K. Sumiyama, T. Hihara, and T. J. Konno, Scr. Mater. **44**, 1471 (2001).